Published in final edited form as:
Bone. 2010 June ; 46(6): 1652–1660. doi:10.1016/j.bone.2010.02.021.

Regional variations of gender-specific and age-related differences in trabecular bone structure of the distal radius and tibia

Miki Sode[1,2], **Andrew J. Burghardt**[2], **Galateia J. Kazakia**[2], **Thomas M. Link**[2], and **Sharmila Majumdar**[1,2]

[1] Joint Graduate Group in Bioengineering, University of California at San Francisco and Berkeley, San Francisco and Berkeley, California, USA

[2] Musculoskeletal Quantitative Imaging Research Group, Department of Radiology and Biomedical Imaging, University of California at San Francisco, San Francisco, California, USA

Abstract

Regional variation in trabecular structure across axial sections is often obscured by the conventional global analysis, which takes an average value for the entire trabecular compartment. The objective of this study is to characterize spatial variability in trabecular structure within a cross-section at the distal radius and tibia, and gender and age effects using *in vivo* HR-pQCT.

HR-pQCT images of the distal radius and tibia were acquired from 146 healthy individuals aged 20–78 years. Trabecular bone volume fraction (BV/TV), number (Tb.N), thickness (Tb.Th), separation (Tb.Sp), and heterogeneity (Tb.1/N.SD) were obtained in a total of 11 regions – the entire trabecular compartment (the global means), inner, outer, and 8 defined subregions. Regional variations were examined with respect to the global means, and compared between women and men, and between young (20–29 yo) and elderly (65–79 yo) adults.

Substantial regional variations in trabecular bone structure at the distal radius and tibia were revealed (e.g. BV/TV varied −40% to +57% and −59% to +100% of the global means, respectively, for elderly women). The inner-lateral (IL) subregion had low BV/TV, Tb.N, and Tb.Th, and low Tb.Sp and Tb.1/N.SD at both sites; the opposite was true in the outer-anterior (OA) subregion at the distal radius and the outer-medial (OM) and -posterior (OP) subregions at the distal tibia. Gender differences were most pronounced in the inner-anterior (IA) subregion compared to the other regions or the global mean differences at both sites. Trabecular structure correlated with age and differed between young and elderly adults predominantly in the inner-posterior (IP) subregion at the distal radius and in the IL and IA subregions at the distal tibia; on the other hand, it remained unchanged in the OA subregion at the distal radius and in the OM subregion at the distal tibia for both women and men.

This study demonstrated that not only the conventional global analysis can obscure regional differences, but also assuming bone status from that of smaller subregion may introduce a confounding sampling error. Therefore, a combined approach of investigating the entire region, each subregion, and the cortical compartment may offer more complete information.

Corresponding Author: Miki Sode, M.S. Musculoskeletal Quantitative Imaging Research Group, QB3/Byers Hall, Suite 203, 1700 4th Street, University of California, San Francisco, San Francisco, CA 94158, miki.sode@ucsf.edu, Tel: 415-476-3702, Fax: 415-514-9656.

Keywords

Regional variations; Trabecular structure; HR-pQCT; Age; Tibia; Radius

INTRODUCTION

Bone quality is a key component for fracture risk assessment and is determined by complex features such as mineralization, architecture, turnover, collagen cross-link and damage accumulation [1]. Bone strength is determined by the quality and quantity of the mineralized skeletal bone tissue. As bone mineral density (BMD) reflects both bone volume and the degree of mineralization, it has been regarded as a surrogate measure for bone strength. Areal BMD measured using dual x-ray energy absorptiometry (DXA) is primarily used for the routine diagnosis of osteoporosis. However, BMD only explains up to 70% of bone strength [1]. A variety of morphologic parameters have been introduced to quantitatively characterize the structural properties of trabecular bone. These indices include, but not limited to, bone volume-fraction (BV/TV), and metric indices such as trabecular thickness (Tb.Th), number (Tb.N), and separation (Tb.Sp).

With the emergence of high-resolution imaging modalities such as high-resolution peripheral quantitative computed tomography (HR-pQCT), isotropic nominal resolutions of 82 μm can be achieved, enabling *in vivo* assessment of these structural indices for trabecular bone at peripheral sites (specifically at the distal radius and tibia). Their accuracy has been validated against μCT-obtained values [2–4]. Structure indices obtained from HR-pQCT images have also been compared to results of mechanical testing and finite element analysis [5]. In addition, the discriminatory power of HR-pQCT-obtained cortical and trabecular structure indices for disease [6] and fracture [7–9] states has been demonstrated, showing its feasibility as a non-invasive tool for assessing skeletal status.

Density and structural indices of trabecular bone calculated from HR-pQCT images are usually reported as average values for the entire trabecular compartment of interest. However, trabecular density and structure can vary substantially throughout cross-sections of the distal radius and tibia (Figure 1). In fact, Lai et al imaged cores of trabecular bone using μCT and found that trabecular bone in the posterior region of the distal tibia exhibits significantly higher BMD, BV/TV, Tb.N, Tb.Th, and degree of anisotropy, as well as lower Tb.Sp and structure model index compared to the anterior region (all $p < 0.01$) [10]. This is most likely the result of adaptation to the habitual loading pattern [10] as the posterior part of the distal tibia is subject to substantial compressive and shear forces from the ground reaction and internal muscle forces during gait [11,12]. Such regional differences are obscured by global averaging of the entire trabecular compartment. The standard deviation of trabecular separation (denoted either as Tb.1/N.SD or Tb.Sp.SD) is often regarded as a measure of heterogeneity in trabecular bone distribution. While this indicates the degree to which the structure is heterogeneous across the entire trabecular region, it does not provide spatial information.

Regional analysis, by subdividing the HR-pQCT images of the radius and tibia cross-section, provides complementary information about the intrinsic structural heterogeneity of trabecular structure that is related to the underlying biomechanical conditions. We hypothesize that trabecular bone structure varies spatially across the trabecular compartment at the distal radius and tibia, and the degree of differences due to gender and age depend on the region. The objective of this study is to use *in vivo* HR-pQCT to investigate regional variations in trabecular structure at the distal radius and tibia and its differences due to gender and age.

MATERIALS AND METHODS

Subjects

Healthy volunteers aged between 20 to 78 years – 93 women (mean age 48.1 ± 15.8 yr) and 53 men (mean age 44.7 ± 16.7 yr) – were recruited through public fliers posted locally as a part of ongoing effort to build a normative database. Persons with no known disease conditions or received no chronic treatment that may affect bone metabolism were enrolled. All subjects gave written informed consent prior to participation. Out of 93 women, 43 were postmenopausal, who had complete cessation of menses for at least six months prior to entrance into the study. Among a total of 79 individuals with DXA measurements (54 women and 25 men), 15 women and 10 men were classified as osteopenic ($-1 <$ T-score < -2.5 at either L1–L4 or total femur), and 7 women and 3 men were classified as osteoporotic (T-score ≤ -2.5). 46% of the subjects were Asian, followed by 46% Caucasian, reflecting the ethnic composition of San Francisco Bay Area. The study protocol was approved by the University of California San Francisco Committee on Human Research.

HR-pQCT Image Acquisition

The distal radius and tibia of each subject were imaged using an *in vivo* HR-pQCT scanner (XtremeCT, Scanco Medical, Brüttisellen, Switzerland). HR-pQCT image acquisitions were performed by a total of 5 operators over the 3-year course of the study. Each subject's forearm and lower leg were immobilized in corresponding carbon-fiber molds, and fixed to the scanner to minimize motion during acquisition. A 9-mm-long section of the radius and tibia was imaged 9.5 mm and 22.5 mm proximal to the distal endplate, respectively. The non-dominant side was scanned unless there was a history of fracture, in which case, the contra-lateral side was scanned. The x-ray source potential was 60 kVp with a current of 900 μA. A two-dimensional detector containing 3072 × 256 CCD elements was used to acquire 750 projections at a 100 ms integration time per projection. The 12.6 mm field of view was reconstructed across a 1536 × 1536 matrix, yielding 82 μm isotropic voxels. Image acquisition time was 3 minutes per scan. Images were immediately reviewed for motion artifacts and repeated if obvious artifacts were detected. Five radius images were excluded due to motion artifacts despite repeated acquisition. The final dataset consisted of 142 radius and 146 tibiae images. The effective dose was < 3 μSV per measurement [13].

Attenuation values were converted to equivalent hydroxyapatite density (mg HA/cm^3) using a linear relationship based on a phantom containing cylinders of HA-resin mixtures with five different concentrations (0, 100, 200, 400, and 800 mg HA/cm^3) (QRM, Moehrendorf, Germany). For quality control, the linear attenuation values of the phantom were monitored daily.

Analysis

The images were segmented and processed in accordance to the standard patient-style analysis protocol using Image Processing Language (Scanco Medical AG, Brüttisellen, Switzerland) as described elsewhere [6,14–20]. First, a semi-automated edge-defining algorithm was applied to the original grayscale image to contour the periosteal surface. The cortical and trabecular regions were segmented automatically by the analysis protocol as described in detail by Laib et al [17]. The following process for defining subregions was performed on the trabecular mask automatically using Matlab at every slice. The trabecular compartment was first divided into two concentric circular regions (inner and outer subregions), where the area of the inner subregion was 60% of the entire trabecular region. This was consistent with the definition of inner and outer subregions where density measurements were obtained as a part of the standard patient analysis [20,21]. Furthermore, the inner and outer trabecular compartments were divided into angular quadrants at each slice based on the defined reference line. For the radius,

the major axis of the radius cross-section (the longest diameter through the centroid) was used as a reference, as the angle between the major axis of the radius and a line connecting the centroids of the radius and ulna cross-sections moved substantially within a scanned span (~ 3° for radius as opposed to 0.5° for tibia). The quadrants were placed 45° to the reference line. For the tibia, a line connecting the centroids of the tibia and fibula cross-sections was used as a reference. The quadrants were placed 0° to the reference line. A total of 8 subregions resulted, as shown in Figure 2. Each subregion is denoted in a combination of two letters based on anatomic location – I and O denote inner and outer subregions, respectively; and M, P, L, and A denote medial, posterior, lateral and anterior, respectively.

Calculation of the trabecular densitometric and structural indices from HR-pQCT images has been described [17], validated [3,22,23] and employed in many studies [6,14–16,18–20]. In addition to the trabecular bone volume fraction (BV/TV), number (Tb.N), thickness (Tb.Th), separation (Tb.Sp), standard for the patient analysis, the standard deviation of trabecular separation (Tb.1/N.SD, μm) was taken as a measure of heterogeneity in trabecular distribution [24]. These trabecular structural indices were calculated for the entire trabecular compartment (the global means), as well as for the inner, outer, and all 8 subregions. The reproducibility of the trabecular structure indices obtained from *in vivo* HR-pQCT images is ≤ 5.8% at the radius and ≤ 1.5% at the tibia [15].

Statistical analysis

Our dataset contained 125 left and 17 right radii and 125 left and 21 right tibiae but no significant difference in any of the structural indices was detected, therefore, they were pooled. The Shapiro-Wilk W test was used to test the normality of the data. As some indices (especially Tb.Sp and Tb.1/N.SD) were not normally distributed, non-parametric methods were employed for all statistical analyses.

To test the significance of differences in the calculated structural indices in each subregion compared to the global means calculated for the entire trabecular compartment, as well as between 8 subregions, multivariate analysis of variance with the subregion as a repeated measure (RMANOVA) was performed for young and elderly women and men. Subsequently, to identify subregions with significantly different values, post-hoc contrast tests with significance level of $\alpha = 0.005$ were performed in order to control for the experiment-wise probability of making a Type I error. The significance of differences in the structural indices between women and men as well as between young and elderly adults in each region were determined using Mann-Whitney U test with $\alpha = 0.05$. To examine the age-related changes in the trabecular structure indices in each region, linear regression analyses were performed for women and men of all ages and Spearman's coefficient, ρ, was obtained for the correlation. To further illustrate age-related changes in trabecular structure, two subsets of the population were compared: young adults aged 20–29 years and elderly adults aged 65–79 years. This age categorization was used in order to be consistent with previously published work by Khosla et al. and to provide a basis for comparison [16]. The significance of differences in the structural indices between young and elderly adults was determined using Mann-Whitney U test with $\alpha = 0.05$. All statistical tests were performed using JMP (version 7.0, SAS Institute Inc., Cary, NC).

RESULTS

Regional analysis was performed on HR-pQCT images of the distal radius and tibia of 146 healthy individuals (93 women and 53 men). Table 1 summarizes the general description of the entire study population, as well as of the subsets (young and elderly women and men), including DXA-derived anthropometric data (height and weight), HR-pQCT-derived standard

density measurements (vBMD, Tb.vBMD for the entire trabecular region, and the inner and outer subregions).

Regional variations

Table 2 shows the mean values for BV/TV and Tb.N for young and elderly women and men in each region at the distal radius and tibia. Trabecular structure in the inner subregion had lower BV/TV, Tb.N, Tb.Th, and higher Tb.Sp and Tb.1/N.SD compared to the outer trabecular subregion at both distal radius and tibia regardless of gender and age. The mean values for BV/TV and Tb.Th in the outer subregion were approximately twice as the value of the inner subregion at both distal radius and tibia for elderly adults (e.g. BV/TV = 0.163 ± 0.028 in the outer subregion vs. 0.078 ± 0.023 in the inner subregion at the radius for elderly women; $p < 0.001$). Tb.N and Tb.1/N.SD, however, were not significantly different between the inner and outer subregion at both distal radius and tibia regardless of gender and age group.

Figure 3 displays the mean percent differences from the global means in each subregion for all measured parameters for elderly women at their distal radius and tibia. In elderly women, BV/TV ranged from −40% in the IL subregion to +57% in the OP subregion with respect to the global mean at the distal radius, and from −59% in the IL subregion to +100% in the OM subregion at the distal tibia. Low BV/TV, Tb.N, and Tb.Th and high Tb.Sp and Tb.1/N.SD were found in the lateral subregions at the distal radius and in both IL and IA subregions at the distal tibia. In contrast, high BV/TV, Tb.N, and Tb.Th and low Tb.Sp and Tb.1/N.SD were found in the OA subregion at the radius and in both OM and OP subregions at the distal tibia. These trends were spatially similar but with slightly reduced magnitudes at both radius and tibia for young adults and for men.

Gender-specific regional variations

In general, women tended to have lower BV/TV, Tb.N and Tb.Th and higher Tb.Sp and Tb.1/N.SD (e.g. globally, in elderly women, BV/TV, Tb.N and Tb.Th were 15%, 10%, and 7% lower, than elderly men and Tb.Sp and Tb.1/N.SD were 15% and 28% higher, respectively, at the distal radius ($p = NS$ except for BV/TV ($p < 0.05$) (Table 2); with similar to smaller magnitudes at the distal tibia). Gender differences in trabecular structure were stronger between young women and men compared to elderly adults at both distal radius and tibia. The differences in Tb.N, Tb.Sp and Tb.1/N.SD were not significant except between young women and men at the distal tibia.

Figure 4 displays the mean percent differences in the trabecular structure indices for elderly women compared to elderly men in each subregion at the distal radius and tibia. Some regions showed larger differences in trabecular structure between women and men compared to the other regions. For instance, at the distal radius, while BV/TV was 15% lower for elderly women globally ($p = 0.048$), it was 28% lower in the IA subregion ($p < 0.05$) but only 6% lower in the OP subregion ($p = NS$). Similarly at the distal tibia, while BV/TV tended to be lower for elderly women by 14% globally ($p = NS$), it was 29% lower in the IA subregion ($p < 0.05$) but only 0.2% lower in the IP subregion ($p = NS$) (Table 2 and Figure 4).

Age-related variations

Table 3 shows the correlations between the trabecular structure indices and age in each subregion for both women and men. In general, at both distal radius and tibia, BV/TV, Tb.N and Tb.Th correlated negatively with age while Tb.Sp and Tb.1/N.SD correlated positively. Trabecular structure in some regions had stronger and more significant correlations with age compared to the other regions. At the distal radius, the correlations tended to be stronger in the posterior and lateral subregions for women ($|\rho| \leq 0.47$) and in the posterior subregions for men ($|\rho| \leq 0.56$), but weaker in the OA subregion for both women and men ($|\rho| = 0.01–0.12$; all p

= NS) (Table 3). At the distal tibia, the correlations between trabecular structure and age were stronger in the IA subregion for women and IL subregion for men ($|\rho| = 0.22–0.59$; all $p \leq 0.03$), but weaker in the outer subregions for both women and men ($|\rho| = 0.05–0.44$) (Table 3).

In order to further illustrate the difference in regional variation of trabecular bone structure between young and elderly adults, Figure 5 maps the mean percent difference in the trabecular structure indices for elderly women compared to young women in each subregion at the distal radius and tibia. In general, elderly adults had lower BV/TV, Tb.N and Tb.Th and higher Tb.Sp and Tb.1/N.SD compared to young adults. Elderly adults had larger ranges of BV/TV and Tb.Th compared to young adults at both radius and tibia. For instance at the distal radius, BV/TV ranged from −40% in the IL subregion to +57% in the OP subregion with respect to the global mean for elderly women (Figure 3), while it ranged from −33% to +48% in the respective subregions for young women. The ranges of other indices remained comparable between elderly and young adults. Trabecular structure at some regions showed larger differences between young and elderly adults. At the distal radius, while BV/TV tended to be lower for elderly women by 16% globally (p = NS), it was 24% lower in the IP and IL subregions ($p < 0.05$ and NS, respectively) but 3% higher in the OA subregion (p = NS) compared to young women (Table 2 and Figure 5). At the distal tibia, while BV/TV was 25% lower for elderly women globally ($p < 0.001$), it was 42% lower in the IA subregion ($p < 0.001$) but only 15% lower in the OM subregion compared to young women ($p < 0.01$) (Table 2 and Figure 5). Similar patterns and degrees of differences in other trabecular structure indices between young and elderly adults were observed at both radius and tibia (Figure 5).

DISCUSSION

The results of this study highlight the substantial regional variability of trabecular bone structure in the distal radius and tibia, which is obscured by the conventional analysis that reports only the global average value and the standard deviation across the entire trabecular compartment. BV/TV, Tb.N, Tb.Th, Tb.Sp, and Tb.1/N.SD were examined regionally from the HR-pQCT images of the distal radius and tibia of 146 healthy individuals aged from 20–79 years. Our major findings are (1) trabecular bone structure varies dramatically across the cross-section at the distal radius and tibia (e.g. −40% to +57% and −59% to +100% of the global means in BV/TV at the distal radius and tibia, respectively, for elderly women), (2) the gender differences in trabecular structure are more prominent in the IA subregion at the radius as well as tibia compared to the other regions or the global mean differences, and (3) the age-related differences are more prominent in the IP subregion for the radius and in both IL and IA subregions for the tibia compared to the other regions or the global mean differences.

The cross-sectional variations between the subregions observed in this study were substantially larger than the longitudinal variations along the 9-mm span of the scanning section at the distal radius and tibia [25]. For example for elderly women at the distal radius, Tb.N varied from 8% less than the global value (in the IL subregion) to 16% more (in the OM subregion), with the net mean difference of 0.39 mm^{-1}; at the distal tibia, Tb.N varied from 16% less than the global value (in the IA subregion) to 24% more (in the OM subregion) with the net mean difference of 0.59 mm^{-1}. The difference in the global mean of Tb.N between the proximal and distal ends of the scanning section, however, is roughly 0.05 mm^{-1} [25] and 0.17–0.23 mm^{-1} at the distal radius and tibia, respectively [25,26]. One implication of this result is the importance of a careful and standardized procedure for selecting a region to take virtual bone biopsy [27,28] for meaningful comparison across cross-section and between subjects. Assuming bone status of a larger region from that of its smaller subregion using may introduce a confounding sampling error.

One possible explanation for the observed regional variability is the local biomechanical environment, particularly for the tibia as it is a site that is habitually loaded. During gait, the peak force is experienced at the heel [29]. Consequently, substantial compressive and shear forces are imposed on the medial and posterior part of the distal tibia due to the ground reaction force as well as internal muscle forces [11,12,30]. Wolff's law dictates that the bone mass and structure adapt to the mechanical loading patterns it is under [31–35]. In addition, trabecular structural indices correlate well with the tissue-level mechanical property [5,36–39]. As trabecular compartment carries 35–71% of axial loads at this distal section [5], trabecular bone structure is, therefore, expected to have adapted to meet the local biomechanical environment. Indeed, the OM and OP subregions featured greater trabecular bone volume with more numerous, thicker trabeculae with reduced separation and heterogeneity (Figure 3). It also coincides with the area of high compressive strength measured using osteopenetrometer [40], as well as the most frequent sites for stress fracture among runners [41–44].

As an application, the results of regional analysis can provide additional information that was obscured using the conventional global approach. For example, for fall that typically results in a Colles' fracture, the ground reaction force results in a considerable dorsal and lateral compressive to the distal radius [45]. Consequently, strain energy density is elevated at the medial and posterior (dorsal) regions [39]. Coincidentally, the results of this study revealed that trabeculae in the IM and IP subregions are structural vulnerable, particularly for women and elderly adults. Indeed, fracture initiation is observed at these regions under simulated axial and off-axis loading [46], respectively. In combination with fall kinetics measurements, regional analysis can bring underlying local bone property, thereby contributed in elucidating the fracture risk as well as developing preventive strategy.

This study contributed in understanding of the age-related alteration in bone structure by providing spatial and anatomical information. Because the inner trabecular subregion has substantially lower BV/TV and Tb.Th compared to the global mean values regardless of gender, age group or site (Table 2 and Figure 3), it is not a surprise that the age-related deterioration of trabecular structure is more apparent in this region than the outer subregion. The effect is particularly severe for women, as reduced estrogen levels upon menopause leads to loss of bone mass by decreases in BV/TV, Tb.Th, and Tb.N as well as an increase in Tb.Sp [47–53]. Our results are consistent with pronounced bone deterioration in the inner subregion observed in ovariectomized rats [54,55]. For men, on the other hand, age-related alterations in trabecular structure were site-dependent, partially in agreement with Khosla et al [16]. At the distal radius, the age-related decrease in BV/TV was driven by strong overall trabecular thinning particularly in the IP and IL subregions. At the distal tibia, on the other hand, it was driven by trabecular disruption evenly across the trabecular compartment. In fact, there exists disagreement in the literature with regard to the age-related alteration in trabecular bone structure at the distal radius and tibia for men: Mueller et al [7,26] reported significant negative correlations with age for both Tb.N and Tb.Th at the distal radius; Dalzell et al [14] reported a lack of correlation with age for any trabecular structure indices at either site. These discrepancies may be attributed to the complex hormonal interplay involving estrogen [56–58], serum bioavailable estradiol [51], and IGF-I levels [50]. The study design such as *in vivo* versus *ex vivo* images, use of a prototype HR-pQCT [26], and the difference in the study populations, along with many other factors likely contribute to the significant variability in the measures. Clearly, further investigation on the gender difference in age-related changes of trabecular structure at the distal tibia and radius is called for.

There are some limitations in the study design that are worth mentioning. First, the definition of regions employed in this study was arbitrary. However, it was systematic, consistent with anatomical coordinate system, and unaffected by patient positioning. The measurement location was set with a fixed distance (9.2 mm for radius and 22.5 mm for tibia) from the

endplate consistent with the standard *in vivo* protocol regardless of bone length. These locations are known to have variable proportions of cortical and trabecular bone [59] and load sharing [5] for both radius and tibia. As cortical bone is an integral part, regional variations in cortical density and structure are expected. In fact, substantial regional variations in cortical vBMD along the shaft of the tibia measured by the pQCT have been reported [60,61]. Thorough investigation of the regional variation in cortical vBMD, thickness, and area, as well as regional variation in load sharing using finite element analysis on the same dataset using HR-pQCT are currently in progress. In addition, acquiring images at the fixed distance from the endplate disregards individual body size, which has a substantial effect on bone property [1,6]. Sekhon et al [62] reported substantial errors in density measures calculated from HR-pQCT images, related to the cortical geometry and trabecular density. This may be due to beam hardening and scatter. Such effect may confound region-wise comparisons, though this is likely limited to differences between inner and outer sub-regions. The cross-sectional study design in a multi-ethnic population with relatively small sample sizes may compromise the statistical power. In the future, regional differences in age-related changes of trabecular structure at the distal radius and tibia need to be examined in a larger cross-sectional and a longitudinal studies.

In conclusion, this study has provided a basis for understanding the regional variation of trabecular bone structure at the distal radius and tibia. Knowing such intrinsic variability in trabecular structure is critical in interpreting data. As demonstrated in this study, the conventional global analysis can obscure regional differences. Similarly, assuming bone status of a larger region from that of its smaller subregion using virtual bone biopsy [28] may introduce a confounding sampling error. Therefore, a combined approach of investigating the entire region, each subregion, and the cortical compartment may offer more complete information. Applying the proposed regional analysis can provide additional spatial and anatomical information to understanding of the bone status.

Acknowledgments

The authors would like to thank Thelma Munoz and Melissa Guan for subject recruitment, Jing Yi Yu, Ayako Suzuki, and Ben Hyun for HR-pQCT image acquisition, and Dana Carpenter, Janet Goldenstein, and Rich Souza for valuable discussions. This study was supported by NIH RO1 AG17762.

References

1. Osteoporosis prevention, diagnosis, and therapy. NIH Consens Statement 2000;17:1–45.
2. Liu XS, Zhang XH, Sekhon KK, Adam MF, McMahon DJ, Bilezikian JP, Shane E, Guo XE. High-Resolution Peripheral Quantitative Computed Tomography Can Assess Microstructural and Mechanical Properties of Human Distal Tibial Bone. J Bone Miner Res. 2009
3. MacNeil JA, Boyd SK. Accuracy of high-resolution peripheral quantitative computed tomography for measurement of bone quality. Med Eng Phys 2007;29:1096–105. [PubMed: 17229586]
4. Sode M, Burghardt AJ, Nissenson RA, Majumdar S. Resolution dependence of the non-metric trabecular structure indices. Bone 2008;42:728–36. [PubMed: 18276202]
5. MacNeil JA, Boyd SK. Load distribution and the predictive power of morphological indices in the distal radius and tibia by high resolution peripheral quantitative computed tomography. Bone 2007;41:129–37. [PubMed: 17442649]
6. Boutroy S, Bouxsein ML, Munoz F, Delmas PD. In vivo assessment of trabecular bone microarchitecture by high-resolution peripheral quantitative computed tomography. J Clin Endocrinol Metab 2005;90:6508–15. [PubMed: 16189253]
7. Boutroy S, Van Rietbergen B, Sornay-Rendu E, Munoz F, Bouxsein ML, Delmas PD. Finite element analysis based on in vivo HR-pQCT images of the distal radius is associated with wrist fracture in postmenopausal women. J Bone Miner Res 2008;23:392–9. [PubMed: 17997712]
8. Melton LJ 3rd, Riggs BL, van Lenthe GH, Achenbach SJ, Muller R, Bouxsein ML, Amin S, Atkinson EJ, Khosla S. Contribution of in vivo structural measurements and load/strength ratios to the

determination of forearm fracture risk in postmenopausal women. J Bone Miner Res 2007;22:1442–8. [PubMed: 17539738]

9. Radspieler, H.; Frieling, I.; Dambacher, MA.; Neff, M. In Vivo Assessment of 3-Dimensional Bone Micro Architecture with HR-pQCT in Patients With and Without Fractures. 30th Annual Meeting of the American Society for Bone and Mineral Research; Canada: Montréal, Quebéc; 2008.
10. Lai YM, Qin L, Yeung HY, Lee KK, Chan KM. Regional differences in trabecular BMD and micro-architecture of weight-bearing bone under habitual gait loading--a pQCT and microCT study in human cadavers. Bone 2005;37:274–82. [PubMed: 15961358]
11. Sasimontonkul S, Bay BK, Pavol MJ. Bone contact forces on the distal tibia during the stance phase of running. J Biomech 2007;40:3503–9. [PubMed: 17662295]
12. Wehner T, Claes L, Simon U. Internal loads in the human tibia during gait. Clin Biomech (Bristol, Avon) 2009;24:299–302.
13. Laib, A.; Hammerle, S.; Koller, B. A new 100 μm resolution scanner for in vivo 3D-CT of the human forearm and lower leg. 16th International Bone Densitometry Workshop; Annecy, France. 2004.
14. Dalzell N, Kaptoge S, Morris N, Berthier A, Koller B, Braak L, van Rietbergen B, Reeve J. Bone micro-architecture and determinants of strength in the radius and tibia: age-related changes in a population-based study of normal adults measured with high-resolution pQCT. Osteoporos Int 2009;20:1683–94. [PubMed: 19152051]
15. Kazakia GJ, Hyun B, Burghardt AJ, Krug R, Newitt DC, de Papp AE, Link TM, Majumdar S. In vivo determination of bone structure in postmenopausal women: a comparison of HR-pQCT and high-field MR imaging. J Bone Miner Res 2008;23:463–74. [PubMed: 18052756]
16. Khosla S, Riggs BL, Atkinson EJ, Oberg AL, McDaniel LJ, Holets M, Peterson JM, Melton LJ 3rd. Effects of sex and age on bone microstructure at the ultradistal radius: a population-based noninvasive in vivo assessment. J Bone Miner Res 2006;21:124–31. [PubMed: 16355281]
17. Laib A, Hauselmann HJ, Ruegsegger P. In vivo high resolution 3D-QCT of the human forearm. Technol Health Care 1998;6:329–37. [PubMed: 10100936]
18. MacNeil JA, Boyd SK. Improved reproducibility of high-resolution peripheral quantitative computed tomography for measurement of bone quality. Med Eng Phys 2008;30:792–9. [PubMed: 18164643]
19. Sornay-Rendu E, Boutroy S, Munoz F, Delmas PD. Alterations of cortical and trabecular architecture are associated with fractures in postmenopausal women, partially independent of decreased BMD measured by DXA: the OFELY study. J Bone Miner Res 2007;22:425–33. [PubMed: 17181395]
20. Vico L, Zouch M, Amirouche A, Frère D, Laroche N, Koller B, Laib A, Thomas T, Alexandre C. High-Resolution pQCT Analysis at the Distal Radius and Tibia Discriminates Patients With Recent Wrist and Femoral Neck Fractures. Journal of Bone and Mineral Research 2008;23:1741–1750. [PubMed: 18665795]
21. Dalzell N, Kaptoge S, Morris N, Berthier A, Koller B, Braak L, van Rietbergen B, Reeve J. Bone micro-architecture and determinants of strength in the radius and tibia: age-related changes in a population-based study of normal adults measured with high-resolution pQCT. Osteoporos Int. 2009
22. Laib A, Ruegsegger P. Calibration of trabecular bone structure measurements of in vivo three-dimensional peripheral quantitative computed tomography with 28-microm-resolution microcomputed tomography. Bone 1999;24:35–9. [PubMed: 9916782]
23. Muller R, Hildebrand T, Hauselmann HJ, Ruegsegger P. In vivo reproducibility of three-dimensional structural properties of noninvasive bone biopsies using 3D-pQCT. J Bone Miner Res 1996;11:1745–50. [PubMed: 8915782]
24. Laib A, Newitt DC, Lu Y, Majumdar S. New model-independent measures of trabecular bone structure applied to in vivo high-resolution MR images. Osteoporos Int 2002;13:130–6. [PubMed: 11905523]
25. Boyd SK. Site-specific variation of bone micro-architecture in the distal radius and tibia. J Clin Densitom 2008;11:424–30. [PubMed: 18280194]
26. Mueller TL, van Lenthe GH, Stauber M, Gratzke C, Eckstein F, Muller R. Regional, age and gender differences in architectural measures of bone quality and their correlation to bone mechanical competence in the human radius of an elderly population. Bone 2009;45:882–91. [PubMed: 19615477]

27. Gomberg BR, Wehrli FW, Vasilic B, Weening RH, Saha PK, Song HK, Wright AC. Reproducibility and error sources of micro-MRI-based trabecular bone structural parameters of the distal radius and tibia. Bone 2004;35:266–76. [PubMed: 15207767]
28. Wehrli F, Saha P, Gomberg B, Song H. Noninvasive assessment of bone architecture by magnetic resonance micro-imaging-based virtual bone biopsy. Proceedings of the IEEE 2003;91:1520–1542.
29. Cheung JT, Zhang M, Leung AK, Fan YB. Three-dimensional finite element analysis of the foot during standing--a material sensitivity study. J Biomech 2005;38:1045–54. [PubMed: 15797586]
30. Anderson DD, Goldsworthy JK, Shivanna K, Grosland NM, Pedersen DR, Thomas TP, Tochigi Y, Marsh JL, Brown TD. Intra-articular contact stress distributions at the ankle throughout stance phase-patient-specific finite element analysis as a metric of degeneration propensity. Biomech Model Mechanobiol 2006;5:82–9. [PubMed: 16520960]
31. Carter DR, Orr TE, Fyhrie DP. Relationships between loading history and femoral cancellous bone architecture. J Biomech 1989;22:231–44. [PubMed: 2722894]
32. Fernandes P, Rodrigues H, Jacobs C. A Model of Bone Adaptation Using a Global Optimisation Criterion Based on the Trajectorial Theory of Wolff. Comput Methods Biomech Biomed Engin 1999;2:125–138. [PubMed: 11264822]
33. Lanyon LE, Rubin CT. Static vs dynamic loads as an influence on bone remodelling. J Biomech 1984;17:897–905. [PubMed: 6520138]
34. Skedros JG, Baucom SL. Mathematical analysis of trabecular 'trajectories' in apparent trajectorial structures: the unfortunate historical emphasis on the human proximal femur. J Theor Biol 2007;244:15–45. [PubMed: 16949618]
35. Wolff, J. The Law of Bone Remodeling (Das Gesetz der transformation der knochen). Berlin: Springer; 1892.
36. Bevill G, Eswaran SK, Gupta A, Papadopoulos P, Keaveny TM. Influence of bone volume fraction and architecture on computed large-deformation failure mechanisms in human trabecular bone. Bone 2006;39:1218–25. [PubMed: 16904959]
37. Liu XS, Sajda P, Saha PK, Wehrli FW, Guo XE. Quantification of the roles of trabecular microarchitecture and trabecular type in determining the elastic modulus of human trabecular bone. J Bone Miner Res 2006;21:1608–17. [PubMed: 16995816]
38. Mittra E, Rubin C, Gruber B, Qin YX. Evaluation of trabecular mechanical and microstructural properties in human calcaneal bone of advanced age using mechanical testing, muCT, and DXA. J Biomech. 2007
39. Ulrich D, van Rietbergen B, Laib A, Ruegsegger P. Load transfer analysis of the distal radius from in-vivo high-resolution CT-imaging. J Biomech 1999;32:821–8. [PubMed: 10433424]
40. Hvid I, Rasmussen O, Jensen NC, Nielsen S. Trabecular bone strength profiles at the ankle joint. Clin Orthop Relat Res 1985:306–12. [PubMed: 4042494]
41. Bennell KL, Brukner PD. Epidemiology and site specificity of stress fractures. Clin Sports Med 1997;16:179–96. [PubMed: 9238304]
42. Boden BP, Osbahr DC, Jimenez C. Low-risk stress fractures. Am J Sports Med 2001;29:100–11. [PubMed: 11206247]
43. Brukner P, Bradshaw C, Khan KM, White S, Crossley K. Stress fractures: a review of 180 cases. Clin J Sport Med 1996;6:85–9. [PubMed: 8673581]
44. Daffner RH, Pavlov H. Stress fractures: current concepts. AJR Am J Roentgenol 1992;159:245–52. [PubMed: 1632335]
45. Troy KL, Grabiner MD. Asymmetrical ground impact of the hands after a trip-induced fall: experimental kinematics and kinetics. Clin Biomech (Bristol, Avon) 2007;22:1088–95.
46. Troy KL, Grabiner MD. Off-axis loads cause failure of the distal radius at lower magnitudes than axial loads: a finite element analysis. J Biomech 2007;40:1670–5. [PubMed: 17368466]
47. Akhter MP, Lappe JM, Davies KM, Recker RR. Transmenopausal changes in the trabecular bone structure. Bone 2007;41:111–6. [PubMed: 17499038]
48. Brouwers JE, Lambers FM, van Rietbergen B, Ito K, Huiskes R. Comparison of bone loss induced by ovariectomy and neurectomy in rats analyzed by in vivo micro-CT. J Orthop Res 2009;27:1521–7. [PubMed: 19437511]

49. Jiang SD, Shen C, Jiang LS, Dai LY. Differences of bone mass and bone structure in osteopenic rat models caused by spinal cord injury and ovariectomy. Osteoporos Int 2007;18:743–50. [PubMed: 17216554]
50. Khosla S, Melton LJ 3rd, Achenbach SJ, Oberg AL, Riggs BL. Hormonal and biochemical determinants of trabecular microstructure at the ultradistal radius in women and men. J Clin Endocrinol Metab 2006;91:885–91. [PubMed: 16368747]
51. Khosla S, Riggs BL, Robb RA, Camp JJ, Achenbach SJ, Oberg AL, Rouleau PA, Melton LJ 3rd. Relationship of volumetric bone density and structural parameters at different skeletal sites to sex steroid levels in women. J Clin Endocrinol Metab 2005;90:5096–103. [PubMed: 15998772]
52. Riggs BL, Khosla S, Melton LJ 3rd. Sex steroids and the construction and conservation of the adult skeleton. Endocr Rev 2002;23:279–302. [PubMed: 12050121]
53. Yang J, Pham SM, Crabbe DL. High-resolution Micro-CT evaluation of mid- to long-term effects of estrogen deficiency on rat trabecular bone. Acad Radiol 2003;10:1153–8. [PubMed: 14587633]
54. Bagi CM, Ammann P, Rizzoli R, Miller SC. Effect of estrogen deficiency on cancellous and cortical bone structure and strength of the femoral neck in rats. Calcif Tissue Int 1997;61:336–44. [PubMed: 9312205]
55. Ito M, Nishida A, Nakamura T, Uetani M, Hayashi K. Differences of three-dimensional trabecular microstructure in osteopenic rat models caused by ovariectomy and neurectomy. Bone 2002;30:594–8. [PubMed: 11934651]
56. Khosla S, Melton LJ 3rd, Riggs BL. Clinical review 144: Estrogen and the male skeleton. J Clin Endocrinol Metab 2002;87:1443–50. [PubMed: 11932262]
57. Khosla S, Atkinson EJ, Dunstan CR, O'Fallon WM. Effect of estrogen versus testosterone on circulating osteoprotegerin and other cytokine levels in normal elderly men. J Clin Endocrinol Metab 2002;87:1550–4. [PubMed: 11932280]
58. Gennari L, Nuti R, Bilezikian JP. Aromatase activity and bone homeostasis in men. J Clin Endocrinol Metab 2004;89:5898–907. [PubMed: 15579733]
59. Schlenker RA, VonSeggen WW. The distribution of cortical and trabecular bone mass along the lengths of the radius and ulna and the implications for in vivo bone mass measurements. Calcif Tissue Res 1976;20:41–52. [PubMed: 1260492]
60. Cooper DM, Ahamed Y, Macdonald HM, McKay HA. Characterising cortical density in the mid-tibia: intra-individual variation in adolescent girls and boys. Br J Sports Med 2008;42:690–5. [PubMed: 18635740]
61. Lai YM, Qin L, Hung VW, Chan KM. Regional differences in cortical bone mineral density in the weight-bearing long bone shaft--a pQCT study. Bone 2005;36:465–71. [PubMed: 15777653]
62. Sekhon K, Kazakia GJ, Burghardt AJ, Hermannsson B, Majumdar S. Accuracy of volumetric bone mineral density measurement in high-resolution peripheral quantitative computed tomography. Bone 2009;45:473–9. [PubMed: 19501201]

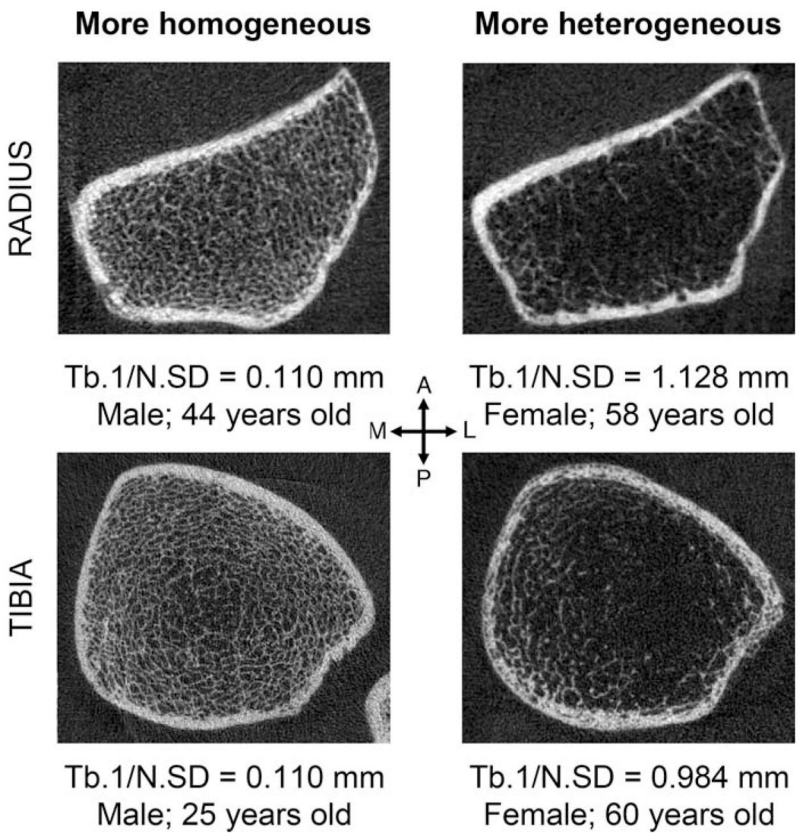

Figure 1.
Representative HR-pQCT images of cross-sections of human distal left radius (top) and tibiae (bottom) with low Tb.1/N.SD (more homogenously distributed) (left) and high Tb.1/N.SD (more heterogeneous distributed) (right). Notice that not only the distribution but also the thickness of trabeculae varies from subregion to subregion.

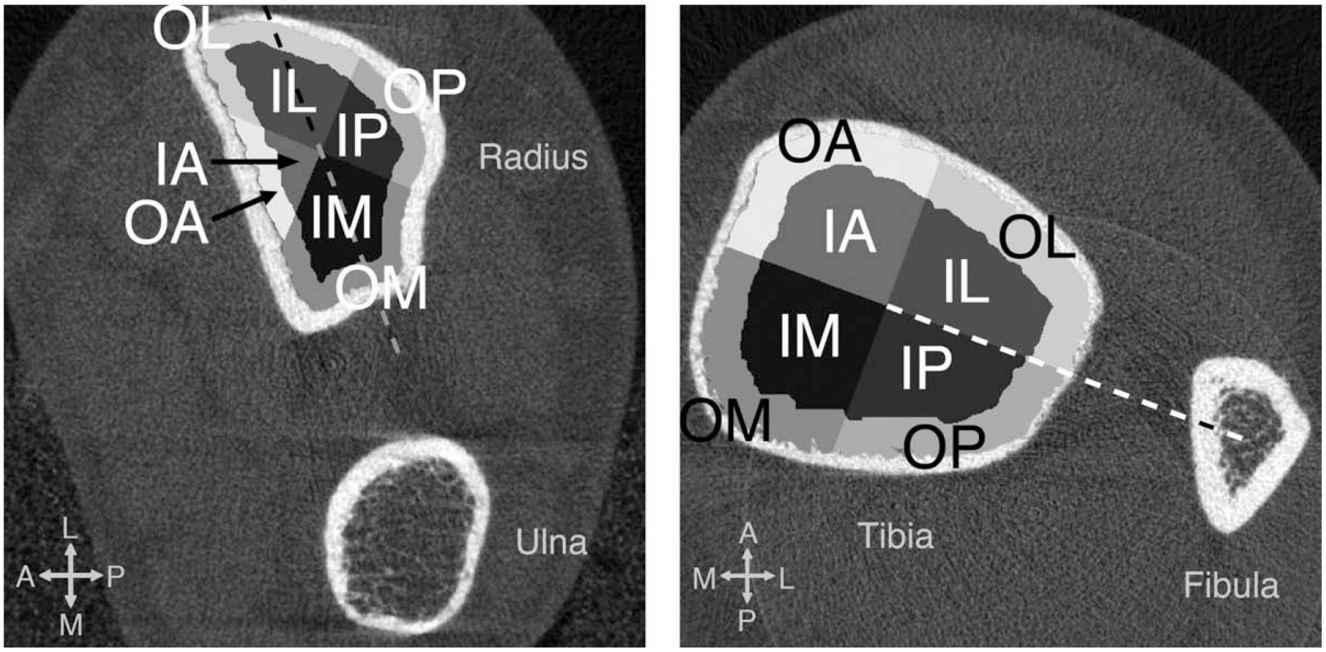

Figure 2.

The region definitions at the distal radius (left) and tibia (right) used in this study. A total of 8 subregions were defined at each slice as follows. The trabecular compartment was divided into two concentric circular regions (inner and outer subregions) where the area of inner subregion was 60% of the entire trabecular region. The trabecular compartment was further divided into angular quadrants based on the defined reference line (dashed). The major axis of the cross-section was used as a reference for radius, and the quadrants were placed 45° to it. The line connecting the centroids of the tibia and fibula cross-sections was used as a reference for tibia, and quadrants were placed 0° to it.

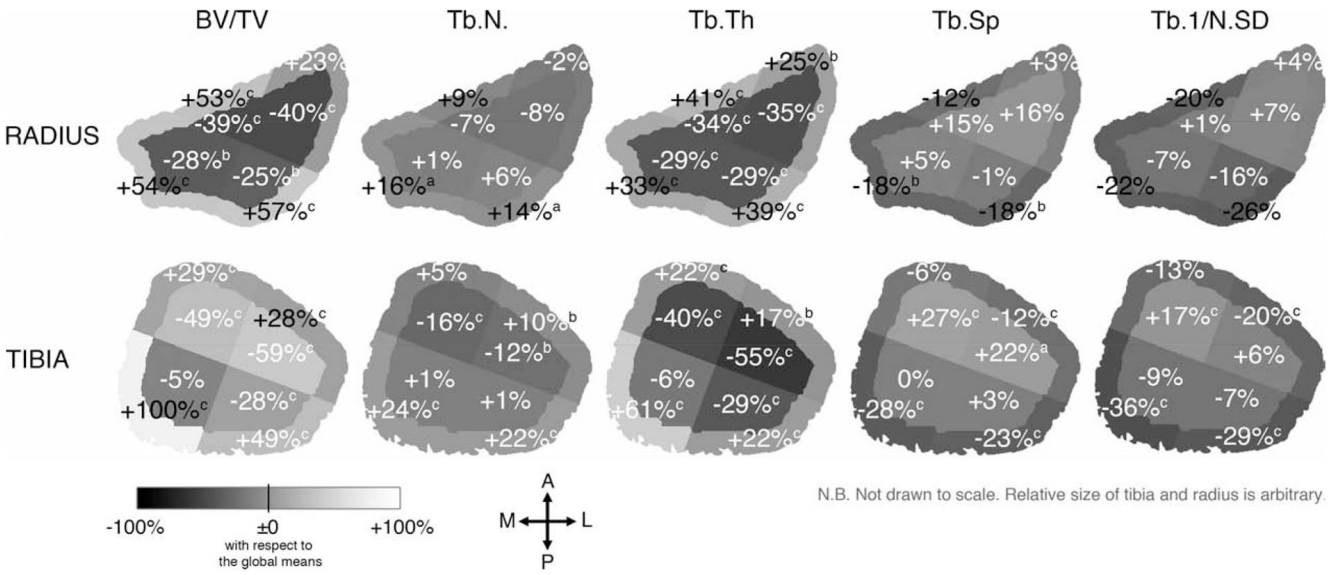

Figure 3.

The mean percent difference from the global means in each subregion for each structure index for elderly women at the distal radius (top) and tibia (bottom). Similar patterns were observed for elderly men and young adults. Significant difference from the global mean with [a] $p < 0.005$; [b] $p < 0.001$ determined by multivariate RMANOVA and post-hoc contrast test.

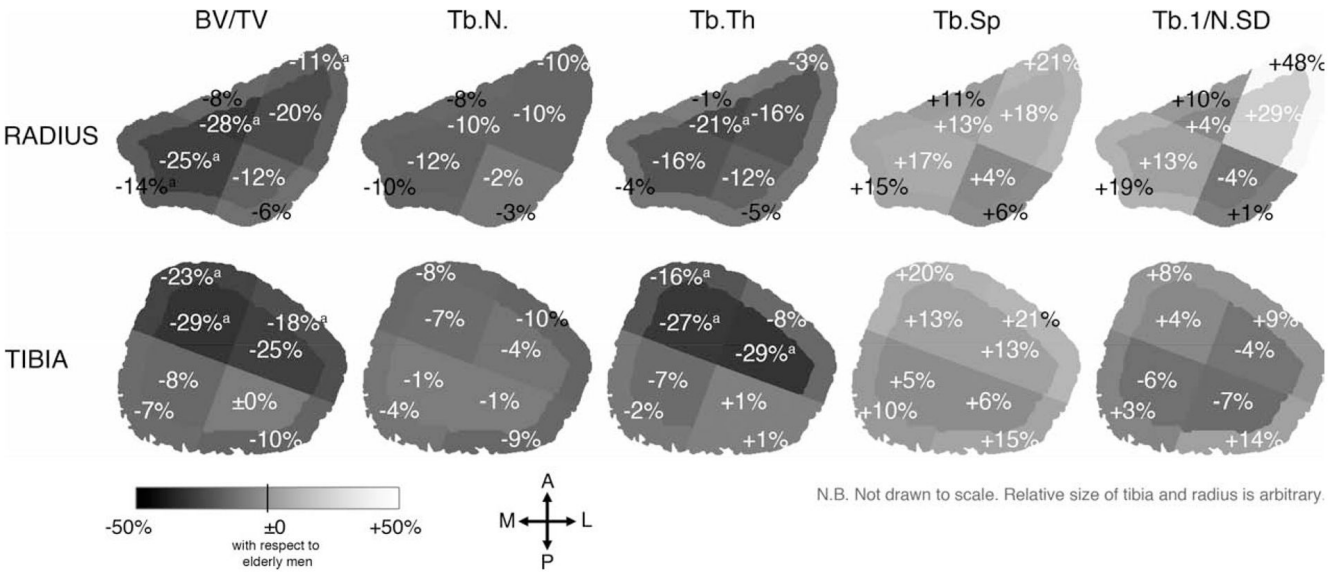

Figure 4.

The mean percent difference in the trabecular structure indices for elderly women (N = 13) compared to elderly men (N = 9) in each subregion at the distal radius (top) and tibia (bottom). Significant difference from elderly men with [a] $p < 0.05$; [b] $p < 0.01$; [c] $p < 0.001$ using Mann-Whitney U test.

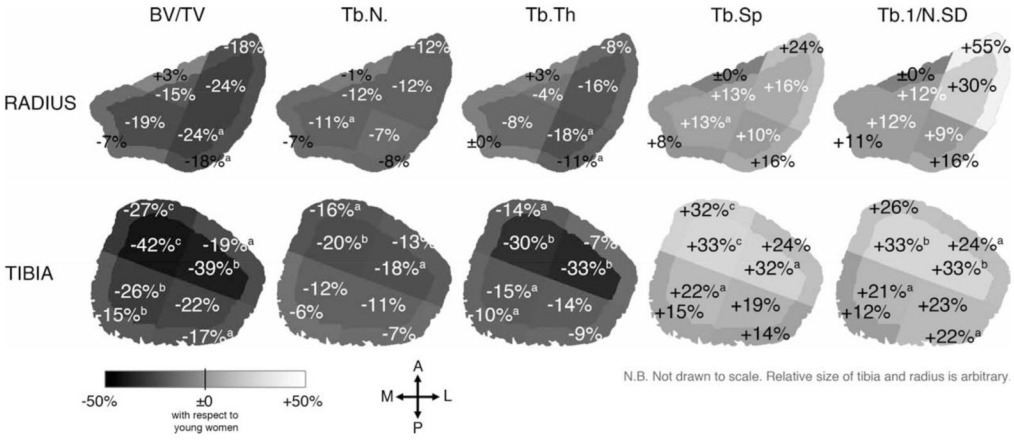

Figure 5.

The mean percent difference in the trabecular structure indices for elderly women (N = 13) compared to young women (N = 17) in each subregion at the distal radius (top) and tibia (bottom). Significant difference from young women with [a] $p < 0.05$; [b] $p < 0.01$; [c] $p < 0.001$ using Mann-Whitney U test.

Table 1

General description of the population – mean ± SD of age, height, weight, BMD, and HR-pQCT-derived bone density indices at the distal radius and tibia for women and men.

	Women			Men			W vs. M (all ages)
	All Ages	**Young (20–9 yrs)**	**Elderly (65–79 yrs)**	**All ages**	**Young (20–29 yrs)**	**Elderly (65–79 yrs)**	**% diff.**
ANTHRO-POMETRIC DATA *							
	53	7	11	25	5	4	
Height [cm]	161.1 ± 6.8	161.8 ± 5.0	156.1 ± 7.0	175.7 ± 7.5	182.4 ± 3.3	168.0 ± 4.9	−8 *c*
Weight [kg]	64.1 ± 13.7	55.6 ± 5.6	60.0 ± 14.4	79.0 ± 15.6	82.4 ± 13.9	71.2 ± 16.8	−19 *c*
RADIUS							
N	87	15	11	55	12	9	
Age [years]	49 ± 16	26 ± 3	72 ± 4	46 ± 16	25 ± 3	70 ± 3	−9
vBMD [mg HA/cm^3]	314.3 ± 62.3	345.2 ± 30.9	284.4 ± 49.6	332.6 ± 51.0	345.4 ± 43.7	306.6 ± 44.9	−5
Tb.vBMD [mg HA/cm^3]	150.4 ± 37.1	162.1 ± 34.0	136.2 ± 31.0	183.8 ± 36.5	205.8 ± 32.1	160.7 ± 17.4	−18 *c*
Tb.vBMD$_{inn}$ [mg HA/cm^3]	108.8 ± 38.7	120.5 ± 36.8	94.9 ± 30.7	145.8 ± 38.8	169.8 ± 33.6	120.5 ± 17.3	−24 *c*
Tb.vBMD$_{out}$ [mg HA/cm^3]	210.4 ± 36.2	221.9 ± 30.8	195.6 ± 35.1	239.0 ± 35.0	257.8 ± 30.8	219.0 ± 20.2	−11 *c*
TIBIA							
N	93	17	13	53	13	9	
Age [years]	48 ± 16	27 ± 3	71 ± 4	45 ± 17	25 ± 3	70 ± 3	+11
vBMD [mg HA/cm^3]	296 ± 60	337.4 ± 45.7	247.3 ± 54.8	317.9 ± 55.5	360.5 ± 45.0	279.5 ± 40.5	−7 *a*
Tb.vBMD [mg HA/cm^3]	155.6 ± 37.8	174.7 ± 29.7	130.6 ± 33.8	184.6 ± 42.1	221.2 ± 35.3	152.7 ± 26.6	−16 *c*
Tb.vBMD$_{inn}$ [mg HA/cm^3]	110.6 ± 38.2	127.6 ± 30.7	86.8 ± 33.6	140.2 ± 43.3	176.2 ± 37.0	102.7 ± 24.7	−21 *c*
Tb.vBMD$_{out}$ [mg HA/cm^3]	221.8 ± 39.4	243.8 ± 31.3	195.1 ± 36.8	250.0 ± 42.3	287.5 ± 35.1	226.5 ± 31.3	−11 *c*

* N.B. Anthropometric data are obtained using Lunar Prodigy (GE Healthcare), and available only for a subset of the population Significant difference in mean values with

a $p < 0.05$;

b $p < 0.01$;

c $p < 0.001$, determined by Mann-Whitney U test.

Table 2

Comparisons of the mean values for BV/TV and Tb.N between young and elderly women and men in each region at the distal radius and tibia.

BV/TV [1]	Women				Men				Women vs. Men			
	Mean ± SD		Y vs. E Differences		Mean ± SD		Y vs. E Differences		Young (20–29 yo)		Elderly (65–79 yo)	
	Young	Elderly	Abs.	%	Young	Elderly	Abs.	%	Abs.	%	Abs.	%
RADIUS												
N	15	11			12	9						
Global	0.135 ± 0.028	0.114 ± 0.026	−0.021	−16	0.172 ± 0.027	0.135 ± 0.014	−0.037	−22 *b*	−0.036	−21 *b*	−0.020	−15 *a*
Inner	0.099 ± 0.030	0.078 ± 0.023	−0.021	−21	0.140 ± 0.029	0.099 ± 0.016	−0.041	−29 *b*	−0.041	−29 *b*	−0.021	−21
Outer	0.184 ± 0.025	0.163 ± 0.028	−0.021	−12	0.214 ± 0.025	0.181 ± 0.019	−0.032	−15 *b*	−0.030	−14 *a*	−0.019	−10 *a*
Subregion IM	0.100 ± 0.031	0.081 ± 0.021	−0.019	−19	0.140 ± 0.033	0.108 ± 0.021	−0.032	−23 *a*	−0.040	−29 *b*	−0.027	−25 *a*
IP	0.114 ± 0.035	0.087 ± 0.029	−0.027	−24 *a*	0.158 ± 0.028	0.099 ± 0.029	−0.059	−38 *b*	−0.045	−28 *b*	−0.012	−12
IL	0.095 ± 0.032	0.072 ± 0.033	−0.023	−24	0.134 ± 0.032	0.090 ± 0.015	−0.045	−33 *c*	−0.039	−29 *a*	−0.018	−20
IA	0.083 ± 0.030	0.070 ± 0.021	−0.013	−15	0.119 ± 0.026	0.096 ± 0.024	−0.023	−19	−0.036	−31 *b*	−0.026	−28 *a*
OM	0.185 ± 0.027	0.172 ± 0.021	−0.013	−7	0.217 ± 0.031	0.199 ± 0.027	−0.018	−8	−0.032	−15 *b*	−0.027	−14 *a*
OP	0.219 ± 0.028	0.179 ± 0.039	−0.040	−18 *a*	0.248 ± 0.023	0.191 ± 0.030	−0.057	−23 *b*	−0.029	−12 *a*	−0.012	−6
OL	0.172 ± 0.030	0.141 ± 0.043	−0.030	−18	0.200 ± 0.027	0.158 ± 0.020	−0.042	−21 *b*	−0.029	−14	−0.017	−11
OA	0.166 ± 0.022	0.170 ± 0.022	+0.004	+3	0.192 ± 0.024	0.185 ± 0.018	−0.007	−4	−0.026	−14 *b*	−0.015	−8
TIBIA												
N	17	13			12	9						
Global	0.146 ± 0.025	0.109 ± 0.028	−0.036	−25 *c*	0.184 ± 0.029	0.127 ± 0.022	−0.057	−31 *c*	−0.020	−15 *b*	−0.018	−14
Inner	0.107 ± 0.025	0.073 ± 0.028	−0.034	−32 *b*	0.147 ± 0.030	0.086 ± 0.021	−0.061	−42 *c*	−0.029	−21 *b*	−0.013	−15
Outer	0.202 ± 0.026	0.162 ± 0.031	−0.040	−20 *c*	0.238 ± 0.030	0.188 ± 0.026	−0.050	−21 *b*	−0.018	−8 *a*	−0.027	−14
Subregion IM	0.140 ± 0.027	0.104 ± 0.026	−0.036	−26 *b*	0.171 ± 0.030	0.113 ± 0.023	−0.058	−34 *c*	−0.018	−11 *a*	−0.009	−8
IP	0.103 ± 0.035	0.080 ± 0.030	−0.023	−22	0.144 ± 0.037	0.080 ± 0.029	−0.063	−44 *b*	−0.029	−22 *a*	−0.000	±0
IL	0.082 ± 0.030	0.050 ± 0.036	−0.032	−39 *a*	0.129 ± 0.035	0.067 ± 0.029	−0.062	−48 *b*	−0.037	−31 *a*	−0.017	−25
IA	0.100 ± 0.026	0.058 ± 0.031	−0.042	−42 *c*	0.146 ± 0.032	0.082 ± 0.018	−0.064	−44 *c*	−0.035	−26 *b*	−0.024	−29 *a*
OM	0.249 ± 0.023	0.211 ± 0.032	−0.038	−15 *b*	0.269 ± 0.036	0.227 ± 0.026	−0.042	−15 *a*	−0.001	0.5	−0.016	−7

BV/TV [1]	Women				Men				Women vs. Men			
	Mean ± SD		Y vs. E Differences		Mean ± SD		Y vs. E Differences		Young (20–29 yo)		Elderly (65–79 yo)	
	Young	Elderly	Abs.	%	Young	Elderly	Abs.	%	Abs.	%	Abs.	%
OP	0.190 ± 0.038	0.159 ± 0.030	−0.032	−17[a]	0.229 ± 0.032	0.176 ± 0.035	−0.053	−23[b]	−0.021	−10[a]	−0.017	−10
OL	0.172 ± 0.036	0.139 ± 0.038	−0.033	−19[a]	0.221 ± 0.032	0.169 ± 0.031	−0.052	−24[b]	−0.032	−16[b]	−0.030	−18[a]
OA	0.191 ± 0.031	0.138 ± 0.038	−0.052	−27[c]	0.233 ± 0.032	0.180 ± 0.030	−0.054	−23[b]	−0.025	−12[a]	−0.041	−23[a]

Tb.N [1/mm]	Women				Men				Women vs. Men			
	Mean ± SD		Y vs. E Differences		Mean ± SD		Y vs. E Differences		Young (20–29 yo)		Elderly (65–79 yo)	
	Young	Elderly	Abs.	%	Young	Elderly	Abs.	%	Abs.	%	Abs.	%
RADIUS												
N	15	11			12	9						
Global	1.88 ± 0.30	1.68 ± 0.26	−0.20	−11	2.03 ± 0.23	1.87 ± 0.26	−0.16	−8	−0.145	−7	−0.189	−10
Inner	1.83 ± 0.33	1.62 ± 0.26	−0.22	−12[a]	1.99 ± 0.23	1.79 ± 0.27	−0.19	−10	−0.158	−8	−0.179	−10
Outer	1.95 ± 0.26	1.77 ± 0.28	−0.18	−9	2.07 ± 0.24	1.96 ± 0.24	−0.11	−5	−0.120	−6	−0.193	−10
Subregion IM	1.88 ± 0.32	1.67 ± 0.25	−0.21	−11[a]	2.06 ± 0.24	1.90 ± 0.32	−0.16	−8	−0.182	−9	−0.226	−12
IP	1.90 ± 0.34	1.77 ± 0.27	−0.14	−7	2.04 ± 0.23	1.80 ± 0.27	−0.24	−12	−0.141	−7	−0.034	−2
IL	1.77 ± 0.36	1.55 ± 0.36	−0.21	−12	1.92 ± 0.25	1.72 ± 0.24	−0.21	−11	−0.157	−8	−0.166	−10
IA	1.75 ± 0.32	1.54 ± 0.24	−0.21	−12	1.88 ± 0.23	1.72 ± 0.35	−0.16	−8	−0.124	−7	−0.176	−10
OM	2.06 ± 0.29	1.93 ± 0.25	−0.14	−7	2.20 ± 0.28	2.15 ± 0.30	−0.05	−2	−0.137	−6	−0.219	−10
OP	2.06 ± 0.23	1.90 ± 0.32	−0.16	−8	2.11 ± 0.19	1.95 ± 0.24	−0.15	−7	−0.044	−2	−0.053	−3
OL	1.88 ± 0.29	1.65 ± 0.39	−0.23	−12	2.00 ± 0.24	1.84 ± 0.22	−0.16	−8	−0.121	−6	−0.189	−10
OA	1.83 ± 0.28	1.80 ± 0.26	−0.03	−1	1.97 ± 0.26	1.96 ± 0.28	−0.01	−1	−0.146	−7	−0.162	−8
TIBIA												
N	17	13			12	9						
Global	1.77 ± 0.23	1.52 ± 0.31	−0.25	−14[a]	2.17 ± 0.41[a]	1.61 ± 0.18	−0.56	−26[b]	−0.396	−18[a]	−0.083	−5
Inner	1.68 ± 0.25	1.41 ± 0.31	−0.27	−16[a]	2.10 ± 0.43[a]	1.46 ± 0.19	−0.64	−30[b]	−0.422	−20[a]	−0.049	−3
Outer	1.94 ± 0.19	1.73 ± 0.32	−0.21	−11[a]	2.29 ± 0.37[a]	1.89 ± 0.18	−0.40	−18[b]	−0.347	−15[a]	−0.156	−8
Subregion IM	1.76 ± 0.23	1.54 ± 0.30	−0.22	−12	2.10 ± 0.42	1.55 ± 0.16	−0.56	−26[b]	−0.346	−17	−0.009	−1
IP	1.73 ± 0.26	1.54 ± 0.35	−0.18	−11	2.21 ± 0.39[a]	1.56 ± 0.22	−0.65	−29[b]	−0.485	−22[b]	−0.019	−1
IL	1.65 ± 0.28	1.36 ± 0.36	−0.29	−18[a]	2.11 ± 0.45[a]	1.42 ± 0.25	−0.69	−33[b]	−0.457	−22[a]	−0.056	−4

Bone. Author manuscript; available in PMC 2011 June 1.

Tb.N [1/mm]	Women				Men				Women vs. Men			
	Mean ± SD		Y vs. E Differences		Mean ± SD		Y vs. E Differences		Young (20–29 yo)		Elderly (65–79 yo)	
	Young	Elderly	Abs.	%	Young	Elderly	Abs.	%	Abs.	%	Abs.	%
IA	1.60 ± 0.29	1.28 ± 0.28	−0.33	−20[b]	2.01 ± 0.47	1.36 ± 0.19	−0.64	−32[b]	−0.403	−20	−0.089	−7
OM	1.98 ± 0.15	1.87 ± 0.32	−0.11	−6	2.24 ± 0.38[a]	1.96 ± 0.13	−0.28	−13[a]	−0.256	−11[a]	−0.081	−4
OP	1.99 ± 0.22	1.85 ± 0.32	−0.14	−7	2.45 ± 0.37[a]	2.03 ± 0.19	−0.42	−17[b]	−0.461	−19[b]	−0.178	−9
OL	1.91 ± 0.25	1.67 ± 0.37	−0.24	−13	2.33 ± 0.37[a]	1.86 ± 0.23	−0.47	−20[b]	−0.420	−18[a]	−0.190	−10
OA	1.90 ± 0.24	1.60 ± 0.35	−0.30	−16[a]	2.17 ± 0.37	1.74 ± 0.18	−0.43	−20[b]	−0.268	−12	−0.138	−8

Significant difference in mean values with

[a] $p < 0.05$;

[b] $p < 0.01$;

[c] $p < 0.001$ using Mann-Whitney U test.

For graphical display of the differences in all examined structural indices at each region for elderly women compared to elderly men, see Figure 4. Similarly, for graphical display of the difference in structural indices at each region for elderly women compared to young women, see Figure 5.

Bone. Author manuscript; available in PMC 2011 June 1.

Table 3

Spearman's correlation coefficients for the trabecular structure indices and age in each region for women (N = 93) and men (N = 53).

Spearman's	BV/TV		Tb.N		Tb.Th		Tb.Sp		Tb.1/N.SD	
ρ	Women	Men	Women	Men	Women	Men	Women	Men	Women	Men
RADIUS										
Global	−0.33[b]	−0.52[c]	−0.21	−0.19	−0.30[b]	−0.35[b]	0.24[a]	0.29[a]	0.21	0.27[a]
Inner	−0.30[b]	−0.51[c]	−0.24[a]	−0.22	−0.29[b]	−0.44[c]	0.25[a]	0.29[a]	0.21[a]	0.28[a]
Outer	−0.37[c]	−0.44[c]	−0.15	−0.13	−0.28[b]	−0.32[a]	0.19	0.24	0.13	0.20
Subregion IM	−0.23[a]	−0.40[b]	−0.19	−0.20	−0.19	−0.35[b]	0.21	0.26	0.17	0.25
IP	−0.35[c]	−0.56[c]	−0.17	−0.22	−0.39[c]	−0.53[c]	0.21	0.36[b]	0.21	0.30[a]
IL	−0.33[b]	−0.50[c]	−0.23[a]	−0.23	−0.34[b]	−0.46[c]	0.25[a]	0.30[a]	0.18	0.30[a]
IA	−0.14	−0.35[b]	−0.21	−0.17	−0.09	−0.29[a]	0.20	0.22	0.16	0.22
OM	−0.24[a]	−0.27[a]	−0.09	−0.11	−0.15	−0.18	0.12	0.18	0.06	0.16
OP	−0.43[c]	−0.56[c]	−0.11	−0.15	−0.47[c]	−0.47[c]	0.19	0.32[a]	0.06	0.23
OL	−0.41[c]	−0.46[c]	−0.21	−0.16	−0.37[c]	−0.38[b]	0.26[a]	0.30[a]	0.21[a]	0.28[a]
OA	0.05	−0.12	0.02	−0.03	0.01	−0.12	−0.02	0.06	−0.08	0.11
TIBIA										
Global	−0.42[c]	−0.61[c]	−0.20[a]	−0.51[c]	−0.38[c]	−0.17	0.24[a]	0.56[c]	0.24[a]	0.55[c]
Inner	−0.39[c]	−0.62[c]	−0.21[a]	−0.53[c]	−0.43[c]	−0.37[b]	0.24[a]	0.57[c]	0.23[a]	0.54[c]
Outer	−0.43[c]	−0.53[c]	−0.17	−0.44[b]	−0.30[b]	−0.14	0.22[a]	0.50[c]	0.17	0.51[c]
Subregion IM	−0.39[c]	−0.54[c]	−0.17	−0.48[c]	−0.38[c]	−0.23	0.22[a]	0.52[c]	0.20	0.50[c]
IP	−0.28[b]	−0.58[c]	−0.13	−0.51[c]	−0.31[b]	−0.37[b]	0.16	0.57[c]	0.17	0.54[c]
IL	−0.33[b]	−0.59[c]	−0.22[a]	−0.53[c]	−0.35[c]	−0.42[b]	0.23[a]	0.54[c]	0.22[a]	0.53[c]
IA	−0.40[c]	−0.57[c]	−0.26[a]	−0.48[c]	−0.39[c]	−0.32[a]	0.28[b]	0.50[c]	0.25[a]	0.48[c]
OM	−0.35[c]	−0.41[b]	−0.10	−0.36[b]	−0.32[b]	−0.16	0.15	0.42[b]	0.05	0.44[c]
OP	−0.33[b]	−0.46[c]	−0.10	−0.42[b]	−0.30[b]	−0.17	0.14	0.49[c]	0.19	0.51[c]
OL	−0.30[b]	−0.54[c]	−0.17	−0.45[c]	−0.22[a]	−0.15	0.20	0.52[c]	0.19	0.52[c]
OA	−0.42[c]	−0.53[c]	−0.21[a]	−0.42[b]	−0.30[b]	−0.12	0.25[a]	0.50[c]	0.12	0.49[c]

Significant correlation with age (ρ) with

[a] $p < 0.05$;

[b] $p < 0.01$; and

[c] $p < 0.001$.